AGU ADVANCING EARTH AND SPACE SCIENCE

Geophysical Research Letters

RESEARCH LETTER
10.1029/2022GL101953

Solar Cycle and Long-Term Trends in the Observed Peak of the Meteor Altitude Distributions by Meteor Radars

E. C. M. Dawkins[1,2], G. Stober[3], D. Janches[1], J. D. Carrillo-Sánchez[1,2], R. S. Lieberman[1], C. Jacobi[4], T. Moffat-Griffin[5], N. J. Mitchell[5,6], N. Cobbett[5], P. P. Batista[7], V. F. Andrioli[7,8], R. A. Buriti[9], D. J. Murphy[10], J. Kero[11], N. Gulbrandsen[12], M. Tsutsumi[13,14], A. Kozlovsky[15], J. H. Kim[16], C. Lee[16], and M. Lester[17]

[1]ITM Physics Laboratory, NASA Goddard Space Flight Center, Greenbelt, MD, USA, [2]Department of Physics, Catholic University of America, Washington, DC, USA, [3]Microwave Physics, Institute of Applied Physics, University Bern, Bern, Switzerland, [4]Institute for Meteorology, Leipzig University, Leipzig, Germany, [5]British Antarctic Survey, Cambridge, UK, [6]University of Bath, Bath, UK, [7]National Institute for Space Research (INPE), São José dos Campos, Brazil, [8]China-Brazil Joint Laboratory for Space Weather, NSSC/INPE, São José dos Campos, Brazil, [9]Department of Physics, Federal University of Campina Grande, Campina Grande, Brazil, [10]Australian Antarctic Division, Kingston, TAS, Australia, [11]Swedish Institute of Space Physics (IRF), Kiruna, Sweden, [12]Tromsø Geophysical Observatory, UiT—The Arctic University of Norway, Tromsø, Norway, [13]National Institute of Polar Research, Tachikawa, Japan, [14]The Graduate University for Advanced Studies (SOKENDAI), Tokyo, Japan, [15]Sodankylä Geophysical Observatory, University of Oulu, Oulu, Finland, [16]Division of Atmospheric Sciences, Korea Polar Research Institute, Incheon, S. Korea, [17]Department of Physics and Astronomy, University of Leicester, Leicester, UK

Key Points:

- Use of geographically diverse meteor radar peak detection altitudes to assess long-term and 11-year solar cycle (SC) trends in mesopause region
- The altitude of observed peak meteor height has decreased over time at all locations, regardless of latitude and data set
- Positive correlation at low- and mid-latitude locations with the 11-year SC, but more complex response at high-latitudes

Supporting Information:

Supporting Information may be found in the online version of this article.

Correspondence to:

E. C. M. Dawkins,
erin.dawkins@nasa.gov

Citation:

Dawkins, E. C. M., Stober, G., Janches, D., Carrillo-Sánchez, J. D., Lieberman, R. S., Jacobi, C., et al. (2023). Solar cycle and long-term trends in the observed peak of the meteor altitude distributions by meteor radars. *Geophysical Research Letters*, *50*, e2022GL101953. https://doi.org/10.1029/2022GL101953

Received 3 NOV 2022
Accepted 12 DEC 2022

Abstract

The mesosphere/lower thermosphere (MLT, 80–100 km) region is an important boundary between Earth's atmosphere below and space above and may act as a sensitive indicator for anthropogenic climate change. Existing observational and modeling studies have shown the middle atmosphere and the MLT is cooling and contracting because of increasing greenhouse gas emissions. However, trend analyses are highly sensitive to the time periods covered, their length, and the measurement type and methodology used. We present for the first time the linear and 11-year solar cycle responses in the meteor ablation altitude distributions observed by 12 meteor radars at different locations. Decreasing altitudes were seen at all latitudes (linear trends varying from −10.97 to −817.95 m dec^{-1}), and a positive correlation with solar activity was seen for most locations. The divergence of responses at high latitudes indicates an important and complex interplay between atmospheric changes and dynamics at varying time scales.

Plain Language Summary

High up in our atmosphere lies the mesosphere/lower thermosphere region (80–100 km); an important transition zone between the atmosphere below and space above. Existing studies indicate that this region is changing (cooling and contracting) in response to increasing greenhouse gas emissions, quite unlike the net warming we see near the surface. However these trend studies are often highly sensitive to choice and length of time period covered, and the methodology and type of measurements used. Here we present for the first time a self-consistent methodology applied to 12 different meteor radar station datasets located at a diverse range of latitudes. We looked at changes in the mean peak altitude of individual meteoroid detections, and found decreasing peak altitudes at all locations examined (linear trends varying from −10.97 to −817.95 m decade^{-1}) consistent with a global cooling and contracting of the upper atmosphere. We also examined the response to the 11-year solar cycle and found a positive correlation with solar activity (i.e., increased meteoroid peak altitudes during solar maximum, and vice versa) for low and mid-latitude locations. However we found an anti-correlation at high latitudes suggestive of an important and complex interplay between atmospheric changes and dynamics at varying time scales.

1. Introduction

There has been an increasing interest in how our whole atmosphere is changing ever since modeling work by Roble and Dickinson (1989) demonstrated the global mean mesospheric temperatures would cool by ~10 K under a doubled-CO_2 emission scenario. While it is commonly understood that greenhouse gases (GHGs) act as radiative heaters in Earth's atmosphere, these same gases act as net radiative coolers in the mesosphere and lower thermosphere (MLT) region, as re-emitted heat energy is simply lost to space due to lower air density, rather than being re-absorbed by adjacent molecules (e.g., Roble, 1995).

Observational and modeling studies indicate the MLT is responding to increasing GHG emissions (including water vapor) as well as to changes in stratospheric O_3 concentrations through time. Cooling trends have been reported (Laštovička, 2017, 2021; Plane et al., 2015), along with decreases in MLT and thermospheric neutral density (Brown et al., 2021; Stober et al., 2014), and changes in the ionospheric E layer heights (Bremer, 2008). Additionally, DeLand et al. (2007), DeLand and Thomas (2019), and Shettle et al. (2009) reported an increase in the occurrence, frequency, and brightness of polar mesospheric clouds (PMCs), themselves a sensitive indicator of climate change as they occur under specific conditions of both temperature and water vapor content (Collins et al., 2021). The predicted temperature changes in the middle atmosphere (up to 2–3 K dec^{-1} cooling) are much larger than the warming at the surface (~0.5 K dec^{-1} during the last 50 years (IPCC, 2021)), indicating that the middle and upper atmosphere are very sensitive and could act as an early warning signal for future climate change.

While most studies indicate cooling trends in the middle and upper atmosphere, the sign and magnitude of these trends is not always consistent, particularly within the highly uncertain mesopause region ranging from ~87 km during summer up to 100 km during wintertime (Plane et al., 2015). Derived trends often differ due to differences in the period covered, length of time series, measurements used, and analysis methodologies (Das, 2021; Hervig et al., 2019).

Another significant source of variability in the MLT is the 11-year solar cycle (SC). We are currently in SC 25 and approaching the next solar maximum (last occurring 2014). As well as intra-SC variability, variation occurs between successive SCs, with SC 24 being considerably quieter than the preceding cycle 23 (~1997–2008/2009). The impact of the 11-year SC on the MLT region is complex. Temperature trends are generally positively correlated with SC (higher temperatures during solar maximum conditions) with a stronger response at high latitudes (Beig, 2011; Bizuneh et al., 2022; Dalin et al., 2020; Dawkins et al., 2016; Forbes et al., 2014; Marsh et al., 2007; Remsberg, 2008; Xu et al., 2007; Zhao et al., 2020, 2021).

Thermospheric densities are anticorrelated with solar activity as nitric oxide, NO, acting as an infrared cooler at these MLT altitudes similar to CO_2, has a factor 3–4 increase in density during solar maximum conditions from increased production due to enhanced photoelectric impact ionization, dissociation of nitrogen and subsequent interaction with molecular oxygen (Li et al., 2018; Mlynczak et al., 2010; Qian et al., 2011). Upper mesospheric water vapor abundance is also anticorrelated with solar activity, due to increased photolysis of H_2O from the enhanced Lyman-alpha flux during solar maxima (Hartogh et al., 2013; Nedoluha et al., 2009; Remsberg et al., 2018). As a result, PMC frequency and brightness are also anticorrelated with 11-year SC activity (Dalin et al., 2020; DeLand et al., 2007; Shettle et al., 2009). However, Hervig et al. (2019) has noted stronger anticorrelations between PMCs and SC activity prior to 2002. The dynamical response to the SC (e.g., zonal wind, semidiurnal tides, and gravity wave activity) is very mixed and varies significantly seasonally with both altitude and latitude (Liu et al., 2017; Wilhelm et al., 2019).

Relatively few studies have examined the implications of a changing atmospheric composition on mesopause altitude. To date, most work has been performed using models, with Akmaev et al. (2006), Lübken et al. (2009, 2013), and Lübken and Berger (2011) finding decreases in geometric heights at MLT pressure levels attributable to hydrostatic cooling associated with increasing GHG emission. Empirical studies are limited: observations have shown a decrease of low-frequency radio wave reflection heights in the MLT region (Bremer & Peters, 2008; Kürschner & Jacobi, 2003; Lübken et al., 2013). Jacobi (2014) analyzed meteor mean altitudes at 51.3°N during one SC and found a trend of −560 m dec^{-1}, while Lima et al. (2015) reported a meteor peak height trend of −380 dec^{-1} at 22.7°S. An earlier study at the same location by Clemesha and Batista (2006) reported changes in the meteor centroid altitude between −300 and −800 m dec^{-1} between 2000 and 2005. Yuan et al. (2019) who analyzed sodium lidar data at two mid-latitude locations (~41°N, ~42°N) between 1990 and 2018 reported mesopause altitude trends of -450 ± 90 m dec^{-1} at 97 km during non-summer months and -130 ± 160 m dec^{-1} at 92 km during non-winter months, respectively. Bailey et al. (2021) conducted the first study to assess how geometric altitude changes in a time series constructed from three satellite instruments (HALOE, TIMED/SABER and SOFIE) and demonstrated altitudes in the polar mesopause were decreasing at a rate of 150–200 m dec^{-1}. However, the results were limited to polar regions, due to spatial and temporal limitations imposed by the latitudinal coverage of the respective satellites, as well as the inherent challenge of combined observational time series from different satellites. A recent study by Mlynczak et al. (2022) analyzed SABER mesospheric geopotential height measurements

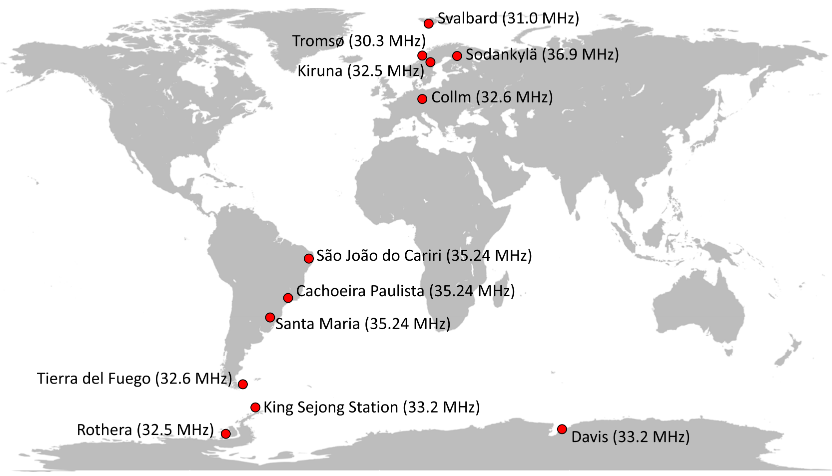

Figure 1. Operating frequencies and latitudinal coverage provided by the 12 meteor radar datasets used in this work.

from 2002 to 2019, averaged between ±55°, and found an average change of −354.6 m at 105 km (approximately equivalent to −197 m dec^{-1}), attributable to increasing CO_2.

We report the first empirical look at how altitudes in the poorly understood mesopause region are changing globally, using a network of meteor radars covering a broad range of latitudes. We describe how the peak observed meteor altitudes are extracted from the individual meteor observations of 12 independent meteor radar stations. A multilinear regression model is applied to the respective observed meteor altitude time series to extract the linear and 11-year SC responses. We relate these trends to latitude to assess how the Earth's complex middle and upper atmosphere is changing.

2. Methodology

Meteor radars detect individual meteor trail echoes, each caused by the atmospheric entry of a meteoroid, with typical diameters between 100 and 1000 μm, and entry velocity of 11–72 km s^{-1}. The observed Doppler shift of a meteor trail echo is caused by the meteor plasma drifting with the atmospheric wind. Meteor trail radars have been used to study atmospheric dynamics in the MLT region since the 1950s (Greenhow, 1952), with an increasing number of standardized radars since the late 1990s (Andrioli et al., 2013; Chau et al., 2021; de Wit et al., 2014; Fritts et al., 2010; Jacobi et al., 2007; Liu et al., 2013; Stober et al., 2022). Individual meteors enter the meteor radar field-of-view and the altitude of the observed meteor is determined using interferometric techniques (Hocking et al., 2001).

We collected meteor observations from 12 different meteor radar stations extending across a broad variety of different latitudes as presented in Figure 1; Svalbard (hereafter SVA, 77.9°N 20.8°E), Tromsø (TRO, 69.4°N 19.1°E), Kiruna (KIR, 67.5°N 20.3°E), Sodankylä (SOD, 67.4°N 26.6°E), Collm (COL, 51.3°N 13.0°E), São João do Cariri (CAR, 7.4°S 36.5°W), Cachoeira Paulista (CPa, 22.7°S 45.0°W), Santa Maria (SMa, 29.7°S 53.7°W) Tierra Del Fuego (TdF, 53.8°S 67.8°W), King Sejong (KSS, 62.0°S 58.0°W), Rothera (ROT, 67.3°S 68.1°W), and Davis (DAV, 68.6°S 78.0°E). The majority of these datasets consist of 15–20 years' worth of consecutive measurements (full data periods are provided Table S1 in Supporting Information S1). The exception is SMa (2004–2012, ∼8 years), and there are data gaps for CAR (2004–2009, 2018–2021, covering ∼10 years in total), CPa (1999–2008, 2012–2021, ∼19 years) and ROT (2004–2013, 2018–2022, ∼15 years). SMa and CAR were included in this analysis as they nearly cover a full 11-year SC and represent important low-latitude locations. Data between 2014 and 2017 for ROT exists but is excluded due to known interference with the nearby TdF station which was using the same operating frequency resulting in contamination of the ROT signal.

The operating frequencies of the meteor radars included in this work (Figure 1) are sufficiently similar resulting in individual meteoroids of the same size (diameter) distribution being observed. The altitude at which an individual meteoroid produces a meteor plasma trail detectable by a radar system depends on meteoroid properties such as mass, composition, velocity, and entry angle as well as on the atmospheric density profile. Both the station latitude and corresponding seasonality in entry angle and speed of the incoming meteoroid source populations and their subsequent interactions with the Earth's atmosphere therefore influence the detection altitude (Carrillo-Sánchez et al., 2016; Fentzke & Janches, 2008; Plane et al., 2015). We performed pre-processing steps to minimize the impacts of this shorter-term variability, enabling us to indirectly detect changes in MLT air densities through changes in the peak height of meteoroid ablation.

To find the peak meteor altitude, we form a histogram of all individual meteor altitudes between 83 and 103 km (across the MLT region) in altitude bins of 0.5 km within a given month for each location. A flexible nonparametric curve is fitted to the histogram to determine the most common observed altitude, defined as "peak altitude," at the curve maximum (shown in Figure S1 in Supporting Information S1). From this, we compile a time series of the monthly peak altitudes extending across all years for a given location. We perform some simple filtering of these time series by removing individual months with peak altitudes exceeding 3.5-sigma of the entire data set.

To reduce any issues associated with measurement gaps or shorter temporal variations (seasonal or diurnal) impacting our trend analyses, we consider only a time series of the annual, deseasonalized peak meteor altitude residuals at each location. The deseasonalizing process consists of removing the average seasonal cycle based on multiple years. We remove any variation associated with large-scale dynamics associated with the Quasi-biennial Oscillation (QBO) and the El Niño Southern Oscillation (ENSO) by performing a multi-linear fit of the QBO (at 30 mb) and ENSO sea surface temperature indices to the deseasonalized monthly time series. Further description of this step is provided in Text S1 and Figure S2 in Supporting Information S1. The coefficients of these fits will be described in a future paper. Following these pre-processing steps, we produce annual means of these altitude residuals (after deseasonalizing, and removing QBO and ENSO signals), $y(t)$, and fit a simple multilinear regression model to extract and separate the linear and 11-year SC response components:

$$y(t) = a.t + b.S(t) + c$$

where the dependent t is the time in years, coefficient a is the slope of the linear trend component (units: km yr^{-1}), $S(t)$ is the solar irradiance approximated by the annual mean of the 10.7 cm flux ($F_{10.7}$), coefficient b is the solar coefficient reported in units of 100 solar flux units (100 sfu where 1 sfu = 10^{-22} W m^{-2} Hz^{-1}), and coefficient c is a constant.

3. Results and Discussion

Figure 2 presents a summary of the multilinear regression fits to the annual peak altitude time series for each of the 12 different meteor radar locations. The standard error (SE) of annual data (comprising the SE of all monthly means within that year) and the coefficient of determination (R^2) between the models and data are shown. The proportion of the variation in the annual data time series that the model captures varies across all 12 locations, from a relatively poor model fit at SVA ($R^2 = 0.18$, capturing only 18% of the variation in the data) to a very good model fit at COL ($R^2 = 0.92$, capturing 92% of the variation in the data). For most of the locations the model fit lies within the SE of the respective data times series. For reference, a normalized annual $F_{10.7}$ time series is overlaid for each panel (dashed lines). Qualitatively, there are several clear trends at many of the locations, with an evident linear altitude decrease through time (i.e., SOD, COL), as well as varying degrees of correlation (or anticorrelation) between the observed peak height and the $F_{10.7}$ index (CPa, TdF, DAV).

3.1. Long-Term (Linear) Trends in the Peak Observed Meteor Altitudes

The variation in the linear trend term (derived from coefficient a in the model fit) for all 12 locations is presented in Figure 3a as a function of station latitude. Also shown are the 95% confidence intervals along with the SE bars of the linear trend coefficient. Decreasing trends in altitude are seen at all locations: SVA −10.97 ± 118.40, TRO −261.33 ± 144.51, KIR −544.57 ± 115.81, SOD −362.04 ± 91.75, COL −817.95 ± 67.06, CAR −173.79 ± 134.18, CPa −97.15 ± 118.56, SMa −257.39 ± 213.77, TdF −667.28 ± 288.61, KSS −771.29 ± 184.55, ROT −266.91 ± 100.13, and DAV −527.07 ± 102.58, all in units: m dec^{-1}. The linear trend in % dec^{-1} are also presented in Figure 3a (gray circles), and in Table S2 in Supporting Information S1.

Our peak altitudes reflect net changes in air densities from the MLT down to the Earth's surface; in absolute values, our datasets indicate that the whole atmosphere is shrinking (range: −10.97 ± 118.40 to −817.95 ± 67.06 m dec^{-1})

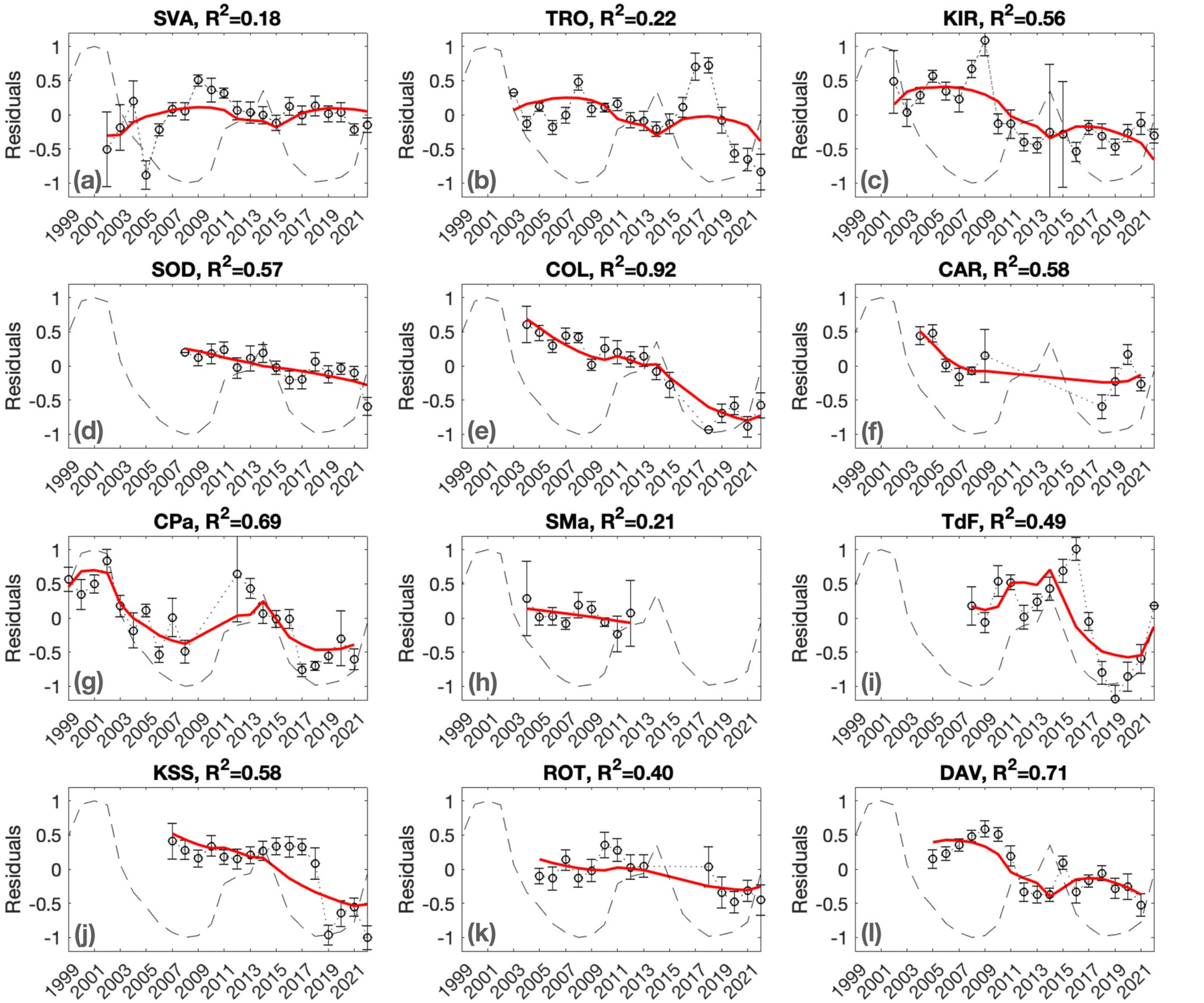

Figure 2. Multilinear regression fits to the annual peak altitude times series for each location; (a) SVA, (b) TRO, (c) KIR, (d) SOD, (e) COL, (f) CAR, (g) CPa, (h) SMa, (i) TdF, (j) KSS, (k) ROT, and (l) DAV. Annual peak observed meteor altitudes are depicted by the black circles with vertical bars corresponding to the SE. The multilinear fit is shown in red and the coefficient of determination (R^2) value between the model and data is presented for each location. A normalized annual solar $F_{10.7}$ time series is overlaid (black dashed lined, in arbitrary units) for reference.

with an average rate of -396.48 ± 139.99 m dec^{-1}. In general, the smallest altitude trends are at low latitudes (range: -97.15 to -173.79 m dec^{-1}), larger negative trends at mid-latitudes (-257.39 to -817.95 m dec^{-1}) with the largest variation at high latitudes (-10.97 to -771.29 m dec^{-1}). The magnitude and sign of these linear trends are broadly consistent with existing empirical altitude studies by Yuan et al. (2019), Bailey et al. (2021), and Mlynczak et al. (2022). Yuan et al. (2019) analyzed two mid-latitude lidar datasets between 1990 and 2018 and found a mesopause altitude trend of -450 ± 90 m dec^{-1} at 97 km and -130 ± 160 m dec^{-1} at 92 km. Bailey et al. (2021) analyzed 29 years of a merged multi-satellite time series within the polar summer mesosphere, reporting a shrinking rate of approximately 150–200 m dec^{-1} throughout the mesosphere, while Mlynczak et al. (2022) found geopotential height changes of -197 m dec^{-1} at ~105 km using 18 years' of SABER satellite measurements averaged between ±55°.

A stronger mid-latitude response relative to lower latitudes is consistent with work by Zhao et al. (2021); they used SABER temperature measurements between ±50°N across 2002–2020 as a function of altitude and found

10.1029/2022GL101953

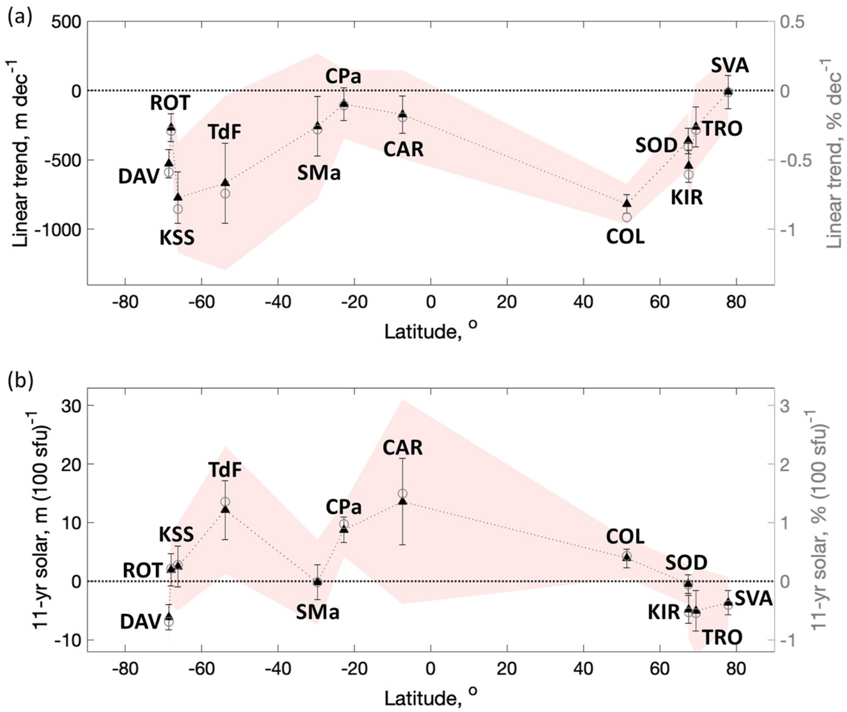

Figure 3. Response coefficients for each of the 12 meteor radar stations as a function of latitude: (a) Linear trends per decade (units: m dec^{-1}), and (b) 11-year SC response (units: m (100 sfu)$^{-1}$). The SE in both the linear trend and 11-year SC responses are indicated by the error bars while the 95% confidence intervals in trend response are indicated by the red shaded areas. The linear and 11-year SC responses are also reported in units of % dec^{-1} and % (100 sfu)$^{-1}$, respectively (right-hand size *y*-axis, gray circles).

larger cooling trends at 50° latitude compared to lower latitudes at altitudes between 85 and 95 km (their Figure 5a). Their earlier study (Zhao et al., 2020) analyzed SABER data for a similar period (2002–2019) across a broader latitude range (between ±83°N) averaging between 80 and 100 km altitude and described large cooling trends at high latitudes above 60° but the 95% confidence intervals were significantly larger than those for other latitudes and all crossed zero. At 80°N, their reported trend was −0.099 K dec^{-1}, with considerable uncertainties extending from approximately −0.29 to +0.9 K dec^{-1}, while at 80°S, they reported a linear response trend of −0.129 K dec^{-1}, with an uncertainty range of approximately −0.3 to +0.03 K dec^{-1}.

At SVA (77.9°N), our most poleward location, the response is quite different from that of the other high-latitude locations (TRO, KIR, SOD, KSS, ROT, DAV), with a near-zero linear trend response (altitude change of −10.97 ± 118.40 m dec^{-1} vs. a range of −261.33 to −771.29 m dec^{-1} for the other locations). While this was the location with the poorest multilinear model fit ($R^2 = 0.18$, Figure 2a), the model fit still lay within the uncertainties of nearly all SVA data points. This near-zero trend may be a reflection of strong dynamical variability within the polar region; including long-term changes in the strength of upward propagating gravity waves during summer or other year-to-year changes in the stability of the polar vortex (Qian et al., 2019), as well as any changes in sudden stratospheric warming events (de Wit et al., 2017; Jacobi et al., 2003; Offerman et al., 2010; Qian et al., 2019; Vincent, 2015; Zhao et al., 2021). Further evidence of the important role of dynamics can be found in the slight hemispheric asymmetry in the linear response with the trends at southern latitudes poleward of 60°S exceeding those poleward of 60°N. This asymmetry is consistent with the findings of Dawkins et al. (2016) that the National Center for Atmospheric Research (NCAR) Whole Atmosphere Community Climate Model (WACCM) 50-year temperatures trends exhibited stronger decadal cooling for the latitude band between 60 and 80°S than that for 60° and 80°N at three different altitudes (−0.60 ± 0.17% dec^{-1} vs. −0.15 ± 0.13% dec^{-1} at 87 km, −0.78 ± 0.14% dec^{-1} vs. −0.32 ± 0.11% dec^{-1} at 90 km, −0.74 ± 0.09% dec^{-1} vs. −0.47 ± 0.10% dec^{-1} at 95 km, for 60°–80°S vs. 60°–80°N, respectively).

Hemispheric asymmetry in the temperature response was also observed by Zhao et al. (2020) and Das (2021) using SABER measurements. Unfortunately, long-term meteor radar data for a low-latitude northern hemisphere location is unavailable, but Sharma et al. (2018), using SABER overpass observations of two low-latitude locations (24.6°N, 21.1°S), were able to demonstrate that the southern hemisphere location had a cooling trend twice that of the northern hemisphere one (-0.14 vs. -0.07 K yr^{-1}). These enhanced southern hemisphere cooling trends (and the subsequent impact of hydrostatic contraction and lowering of altitudes) have been attributed to the changes in the stratospheric circulation: strengthening of the eastward flow in the southern polar vortex because of ozone photochemical depletion and a reduction in the amount of upward propagating planetary waves blocked (French & Burns, 2004; Randel et al., 2017).

Geographic location appears to play an important role in the long-term trend response, again likely because of variability in atmospheric dynamics. Contrasting with our results at CAR and CPa (exhibiting weak trends of -173.79 ± 134.18 m dec^{-1} and -97.15 ± 118.56 m dec^{-1}, respectively), Das (2021) found that the largest cooling trends occurred for equatorial locations. However, they noted significant longitudinal variability, with the largest cooling trends over the Atlantic, Central Pacific, and Northern Indian Ocean locations which they attributed to land-sea differences (stronger cooling events over oceans and weaker cooling over land). This could possibly explain the discrepancies between the strength of the trends at low latitudes reported by Das (2021) and our results for CAR and CPa, both located inland in Brazil.

3.2. Eleven-Year SC Response of the Peak Observed Meteor Altitudes

Figure 3b presents a summary of the 11-year SC responses as a function of station latitude. The response of the peak observed altitude to the 11-year SC ($F_{10.7}$ index, here coefficient b) is mixed and varies between -6.16 and + 13.58 m (100 sfu)$^{-1}$: SVA -3.69 ± 2.09, TRO -5.01 ± 3.49, KIR -4.79 ± 2.38, SOD -0.50 ± 1.59, COL $+3.92 \pm 1.57$, CAR $+13.58 \pm 7.38$, CPa $+8.78 \pm 2.17$, SMa -0.18 ± 2.97, TdF $+12.13 \pm 5.00$, KSS $+2.49 \pm 3.44$, ROT $+1.96 \pm 2.78$, and DAV -6.16 ± 2.17, all in units: m (100 sfu)$^{-1}$. The 11-year SC responses in % (100 sfu)$^{-1}$ are shown in Figure 3b, and in Table S2 in Supporting Information S1. Interpretation of any solar response at SMa is limited as this data set does not cover a full 11-year SC. COL and CPa solar responses agree with those reported using part of the respective datasets within the error bars (Jacobi, 2014; Lima et al., 2015).

There is a coherent latitude response where all low- and mid-latitude station datasets indicate a positive correlation with the 11-year SC, in which higher peak altitudes are associated with solar maximum conditions, and lower peak altitudes occur during solar minimum conditions. This is consistent with enhanced temperatures during solar maximum (because of increased absorption of solar extreme ultraviolet (Solomon et al., 2019)), and the net expansion of the atmosphere, decreasing densities at fixed altitude levels (Stober et al., 2014). Incoming meteoroids encounter more air molecules further up in the atmosphere, and thus ablate higher up in the mesopause (Sparks & Janches, 2009). High-latitude locations such as DAV, KIR, TRO, SOD, and SVA all have negative 11-year SC response components indicating elevated (lower) peak altitudes during solar minimum (maximum) conditions.

The response of the high-latitude atmosphere to the 11-year SC is complex, as seen in the linear trend response, and atmospheric dynamics play an important role (Arnold & Robinson, 1997; Cullens et al., 2016; Ern et al., 2011; Jacobi et al., 2015; Kodera & Kuroda, 2002; Marsh et al., 2007; Vorobeva, 2019). The negative solar trend responses at DAV, KIR, TRO, SOD and SVA indicate that there is significant interplay between these different drivers (zonal wind, semidiurnal tides, gravity wave and planetary wave activity) at high latitudes as atmospheric density, temperature and pressure profiles are closely linked by atmospheric dynamics. Furthermore, these high-latitude stations lie within the auroral oval, thus experiencing enhanced energetic particle precipitation (EPP) during solar maxima; EPP is associated with NO production between 80 and 150 km leading to increased NO infrared cooling (and subsequent hydrostatic contraction) (Smith-Johnson et al., 2022; Solomon et al., 2019).

One curious departure from the behavior of the other high latitude stations is the solar response seen at ROT and KSS; in contrast to their northern hemispheric latitude counterparts (KIR, SOD, and TRO) these stations exhibit a positive correlation with solar activity. Additionally, TdF has a much larger positive solar response compared to its conjugate latitude northern station, COL. These stations are all located within the Southern Andes region, a known gravity-wave hotspot (De Wit et al., 2017; Fritts et al., 2010), which may further point to evidence of a strong dynamical response to the 11-year SC which will be investigated in future work.

4. Conclusions

The response of the MLT region to both long-term changes and the 11-year SC are not fully understood; trend analysis studies are highly sensitive to data continuity, instrument type, analysis methodology and the length and temporal coverage of any time series analyzed (Das, 2021; Forbes et al., 2014; Hervig et al., 2019; Laštovička, 2017). While there have been modeling studies indicating hydrostatic contraction of the upper atmosphere in response to longer term atmospheric changes and the 11-year SC, there are, to our knowledge, only very limited observational studies focusing on altitude changes.

We present the first comprehensive trend analysis using a novel data set consisting of altitude measurements from a network of 12 ground-based meteor radar stations, processed using a self-consistent methodology. The observed meteor altitude distribution peak decreased at all locations, irrespective of latitude (varying from −10.97 to −817.95 m dec^{-1}), providing evidence of a net shrinking whole atmosphere. This is consistent with the work of Yuan et al. (2019), Bailey et al. (2021), Mlynczak et al. (2022), and modeling studies which have demonstrated hydrostatic contraction of the middle and upper atmosphere in response to increasing GHG emissions (Roble and Dickinson, 1989; Akmaev et al., 2006; Lübken & Berger, 2011). The linear response in peak altitude was relatively small at low latitudes and increased toward the mid-latitudes, consistent with work by Zhao et al. (2020, 2021).

At high latitudes, the long-term trends in peak altitude diminish. This contrasts with reports that broadly indicate the strongest trends in temperature, mesospheric O_3, and water vapor occur at high latitudes (Dawkins et al., 2016; Hervig et al., 2016; Zhao et al., 2020), albeit all with larger uncertainties. This behavior, and the hemispheric asymmetry in linear trend responses reported here and in Qian et al. (2017), Sharma et al. (2018), and Das (2021) suggest a role for dynamics, particularly at high latitudes. While we noted a consistent positive correlation between peak altitude and solar activity (higher observed peak altitudes during solar maximum conditions, and decreased altitudes during solar minimum conditions), we found this relationship diverged at high latitudes, again indicative of the strong role of dynamics at these latitudes.

The MLT region remains an important interface between the lower atmosphere and space above, and continuous long-term measurements and consistent trend analysis approaches are vital to monitor and predict changes affecting the whole atmosphere, particularly any non-linear changes in atmospheric dynamics. Future work will utilize this novel meteor radar altitude datasets and seek to further disentangle the processes occurring within this complex mesopause region, particularly the mixed response to the 11-year SC, at shorter timescales (seasonal, diurnal) and within the Southern Andes gravity wave hotspot area.

Acknowledgments

ED, DJ, JDCS, and RSL are supported through the NASA ISFM programs for Heliophysics. GS is a member of the Oeschger Center for Climate Change Research. J-HK and CL were supported by a Korea Polar Research Institute Grant (KOPRI PE22020) from the Ministry of Oceans and Fisheries. CJ acknowledges support by Deutsche Forschungsgemeinschaft (DFG) Grant JA836/43-1. ML acknowledges support from UK Science and Technology Facilities Council Grant ST/W00089X/1. TdF operation is supported by NESC assessment TI-17-01204. ROT and KEP radars were funded through UK Natural Environment Research Council Grants NE/R001391 and NE/R001235/1. CPa, SMa and CAR meteor radars were funded through São Paulo State Research Support Foundation and Brazilian National Research Conseil. DAV operation was supported by Australian Antarctic Science projects 2668, 4025, and 4445. Operation of KIR is provided by the Swedish Space Corporation (SSC) Esrange Space Center.

Data Availability Statement

- The processed data comprising Figures 2 and 3 (and those listed in Table S2 in Supporting Information S1) are made available at https://doi.org/10.5281/zenodo.7374405.

References

Akmaev, R. A., Fomichev, V. I., & Zhu, X. (2006). Impact of middle-atmospheric composition changes on greenhouse cooling in the upper atmosphere. *Journal of Atmospheric and Solar-Terrestrial Physics*, *68*(17), 1879–1889. https://doi.org/10.1016/j.jastp.2006.03.008

Andrioli, V. F., Fritts, D. C., Batista, P. P., & Clemesha, B. R. (2013). Improved analysis of all-sky meteor radar measurements of gravity wave variances and momentum fluxes. *Annales Geophysicae*, *31*(5), 889–908. https://doi.org/10.5194/angeo-31-889-2013

Arnold, N. F., & Robinson, T. R. (1997). Solar cycle changes to planetary wave propagation and their influence on the middle atmosphere circulation. *Annales Geophysicae*, *16*(1), 69–97. https://doi.org/10.1007/s00585-997-0069-3

Bailey, S. M., Thurairajah, B., Hervig, M. E., Siskind, D. E., Russell, J. M., III, & Gordley, L. (2021). Trends in the polar summer mesosphere temperature and pressure altitude from satellite observations. *Journal of Atmospheric and Solar-Terrestrial Physics*, *220*, 105650. https://doi.org/10.1016/j.jastp.2021.105650

Beig, G. (2011). Long-term trends in the temperature of the mesosphere/lower thermosphere region: 2. Solar response. *Journal of Geophysical Research*, *116*(A2). https://doi.org/10.1029/2011JA016766

Bizuneh, C. L., Raju, U. J. P., Nigussie, M., & Santos, C. A. G. (2022). Long-term temperature and ozone response to natural drivers in the mesospheric region using 16 years (2005-2020) of TIMED/SABER observation data at 5-15°N. *Advances in Space Research*, *70*(7), 2095–2111. https://doi.org/10.1016/j.asr.2022.06.051

Bremer, J. (2008). Long-term trends in the ionospheric E and F1 regions. *Annales Geophysicae*, *26*(5), 1189–1197. https://doi.org/10.5194/angeo-26-1189-2008

Bremer, J., & Peters, D. (2008). Influence of stratospheric ozone changes on long-term trends in the meso- and lower thermosphere. *Journal of Atmospheric and Solar-Terrestrial Physics*, *70*(11–12), 1473–1481. https://doi.org/10.1016/j.jastp.2008.03.024

Brown, M. K., Lewis, H. G., Kavanagh, A. J., & Cnossen, I. (2021). Future decreases in thermospheric neutral density in low Earth orbit due to carbon dioxide emissions. *Journal of Geophysical Research: Atmospheres*, *126*(8), e2021JD034589. https://doi.org/10.1029/2021JD034589

Carrillo-Sánchez, J. D., Nesvorný, D., Pokorný, P., Janches, D., & Plane, J. M. C. (2016). Sources of cosmic dust in the Earth's atmosphere. *Geophysical Research Letters*, *43*(23), 11979–11986. https://doi.org/10.1002/2016GL071697

Chau, J. L., Marino, R., Feraco, F., Urco, J. M., Baumgarten, G., Lübken, F.-J., et al. (2021). Radar observation of extreme vertical drafts in the polar summer mesosphere. *Geophysical Research Letters*, *48*(16), e2021GL094918. https://doi.org/10.1029/2021GL094918

Clemesha, B., & Batista, P. (2006). The quantification of long-term atmospheric change via meteor ablation height measurements. *Journal of Atmospheric and Solar-Terrestrial Physics*, *68*(17), 1934–1939. https://doi.org/10.1016/j.jastp.2005.12.008

Collins, R. L., Stevens, M. H., Azeem, I., Taylor, M. J., Larsen, M. F., Williams, B. P., et al. (2021). Cloud formation from a localized water release in the upper mesosphere: Indication of rapid cooling. *Journal of Geophysical Research: Space Physics*, *126*(2), e2019JA027285. https://doi.org/10.1029/2019JA027285

Cullens, C. Y., England, S. L., & Garcia, R. R. (2016). The 11 year solar cycle signature on wave-driven dynamics in WACCM. *Journal of Geophysical Research: Space Physics*, *121*(4), 3484–3496. https://doi.org/10.1002/2016JA022455

Dalin, P., Perminov, V., Pertsev, N., & Romejko, V. (2020). Updated long-term trends in mesopause temperature, airglow emissions, and noctilucent clouds. *Journal of Geophysical Research: Atmospheres*, *125*(5), e2019JD030814. https://doi.org/10.1029/2019JD030814

Das, U. (2021). Spatial variability in long-term temperature trends in the middle atmosphere from SABER/TIMED observations. *Advances in Space Research*, *68*(7), 2890–2903. https://doi.org/10.1016/j.asr.2021.05.014

Dawkins, E. C. M., Plane, J. M. C., Chipperfield, M. P., Feng, W., Marsh, D. R., Höffner, J., & Janches, D. (2016). Solar cycle response and long-term trends in the mesospheric metal layers. *Journal of Geophysical Research: Space Physics*, *121*(7), 7153–7165. https://doi.org/10.1002/2016JA022522

DeLand, M. T., Shettle, E. P., Thomas, G. E., & Olivero, J. J. (2007). Latitude-dependent long-term variations in polar mesospheric clouds from SBUV version 3 PMC data. *Journal of Geophysical Research*, *112*, D10. https://doi.org/10.1029/2006/JD007857

DeLand, M. T., & Thomas, G. E. (2019). Extending the SBUV polar mesospheric cloud data record with the OMPS NP. *Atmospheric Chemistry and Physics*, *19*(11), 7913–7925. https://doi.org/10.5194/acp-19-7913-2019

De Wit, R. J., Hibbins, R. E., Espy, P. J., Orsolini, Y. J., Limpasuvan, V., & Kinnison, D. E. (2014). Observations of gravity wave forcing of the mesopause region during the January 2013 major Sudden Stratospheric Warming. *Geophysical Research Letters*, *41*(13), 4745–4752. https://doi.org/10.1002/2014GL060501

De Wit, R. J., Janches, D., Fritts, D. C., Stockwell, R. G., & Coy, L. (2017). Unexpected climatological behavior of MLT gravity wave momentum flux in the lee of the Southern Andes hot spot. *Geophysical Research Letters*, *44*(2), 1182–1191. https://doi.org/10.1002/2016GL072311

Ern, M., Preusse, P., Gille, J. C., Hepplewhite, C. L., Mlynczak, M. G., Russell, J. M., III., & Riese, M. (2011). Implications for atmospheric dynamics derived from global observations of gravity wave momentum flux in stratosphere and mesosphere. *Journal of Geophysical Research*, *116*(D19), D19107. https://doi.org/10.1029/2011JD015821

Fentzke, J. T., & Janches, D. (2008). A semi-empirical model of the contribution from sporadic meteoroid sources on the meteor input function in the MLT observed at Arecibo. *Journal of Geophysical Research*, *113*(A3). https://doi.org/10.1029/2007JA012531

Forbes, J. M., Zhang, X., & Marsh, D. R. (2014). Solar cycle dependence of middle atmosphere temperatures. *Journal of Geophysical Research: Atmospheres*, *119*(16), 9615–9625. https://doi.org/10.1002/2014JD021484

French, W. J. R., & Burns, G. B. (2004). The influence of large-scale oscillations on long-term trend assessment in hydroxyl temperatures over Davis, Antarctica. *Journal of Atmospheric and Solar-Terrestrial Physics*, *66*(6–9), 493–506. https://doi.org/10.1016/j.jastp.2004.01.027

Fritts, D. C., Janches, D., & Hocking, W. K. (2010). Southern Argentina agile meteor radar: Initial assessment of gravity wave momentum fluxes. *Journal of Geophysical Research*, *115*(D19), D19123. https://doi.org/10.1029/2010JD013891

Greenhow, J. S. (1952). A radio echo method for the investigation of atmospheric winds at altitudes of 80 to 100 km. *Journal of Atmospheric and Terrestrial Physics*, *2*(5), 282–291. https://doi.org/10.1016/0021-9169(52)90044-5

Hartogh, P., Jarchow, C., & Hallgren, K. (2013). Investigations of the Solar Influence on Middle Atmospheric water vapour and ozone during the last solar cycle – Analysis of the MPS data set. In F.-J. Lübken (Ed.), *Climate and water of the Sun-Earth system (CAWSES)* (pp. 109–124). Springer Atmospheric Sciences, Springer. https://doi.org/10.1007/978-94-007-4348-9_7

Hervig, M. E., Berger, U., & Siskind, D. E. (2016). Decadal variability in PMCs and implications for changing temperature and water vapor in the upper mesosphere. *Journal of Geophysical Research: Atmospheres*, *121*(5), 2383–2392. https://doi.org/10.1002/2015JD024439

Hervig, M. E., Siskind, D. E., Bailey, S. M., Merkel, A. W., DeLand, M. T., & Russell, J. M., III. (2019). The missing solar cycle response of the polar summer mesosphere. *Geophysical Research Letters*, *46*(16), 10132–10139. https://doi.org/10.1029/2019GL083485

Hocking, W. K., Fuller, B., & Vandepeer, B. (2001). Real-time determination of meteor-related parameters utilizing modern digital technology. *Journal of Atmospheric and Solar-Terrestrial Physics*, *63*(2–3), 155–169. https://doi.org/10.1016/S1364-6826(00)00138-3

Intergovernmental Panel on Climate Change (IPCC). (2021). Summary for policymakers. In V. Masson-Delmotte, P.Zhai, A. Pirani, S. L. Connos, C. Péan, (Eds.), *Climate change 2021: The physical science basis. Contributions of working Group I to the Sixth assessment report of the intergovernmental panel on climate change* (p. 2391). Cambridge University Press. https://doi.org/10.1017/9781009157896.001

Jacobi, C. (2014). Meteor heights during the recent solar minimum. *Advances in Radio Science*, *12*, 61–165. https://doi.org/10.5194/ars-12-161-2014

Jacobi, C., Fröhlich, K., Viehweg, C., Stober, G., & Kürschner, D. (2007). Midlatitude mesosphere/lower thermosphere meridional winds and temperatures measured with meteor radar. *Advances in Space Research*, *39*(8), 1278–1283. https://doi.org/10.1016/j.asr.2007.01.003

Jacobi, C., Kürschner, D., Muller, H. G., Pancheva, D., Mitchell, N. J., & Naujokat, B. (2003). Response of the mesopause region dynamics to the February 2001 stratospheric warming. *Journal of Atmospheric and Solar-Terrestrial Physics*, *65*(7), 843–855. https://doi.org/10.1016/S1364-6826(03)00086-5

Jacobi, C., Lilienthal, F., Geißler, C., & Krug, A. (2015). Long-term variability of mid-latitude mesosphere-lower thermosphere winds over Collm (51°N, 13°E). *Journal of Atmospheric and Solar-Terrestrial Physics*, *136*(B), 174–186. https://doi.org/10.1016/j.jastp.2015.05.006

Kodera, K., & Kuroda, Y. (2002). Dynamical response to the solar cycle. *Journal of Geophysical Researc*h, *107*(D24), ACL5-1–ACL5-12. https://doi.org/10.1029/2002JD002224

Kürschner, D., & Jacobi, C. (2003). Quasi-biennial and decadal variability obtained from long-term measurements of nighttime radio wave reflection heights over central Europe. *Advances in Space Research*, *31*(9), 1701–1706. https://doi.org/10.1016/S0273-1177(03)90465-0

Laštovička, J. (2017). A review of recent progress in trends in the upper atmosphere. *Journal of Atmospheric and Solar-Terrestrial Physics*, *163*, 2–13. https://doi.org/10.1016/j.jastp.2017.03.009

Laštovička, J. (2021). Long-term trends in the upper atmosphere. In W. Wang, Y. Zhang, & L. J. Paxton (Eds.), *Upper atmosphere dynamics and energetics, Ch17, geophysical monograph series*. https://doi.org/10.1002/9781119815631.ch17

Li, Z., Knipp, D., Wang, W., Sheng, C., Qian, L., & Flynn, S. (2018). A comparison study of NO cooling between TIMED/SABER measurements and TIEGCM simulations. *Journal of Geophysical Research: Space Physics*, *123*(10), 8714–8729. https://doi.org/10.1029/2018JA025831

Lima, L. M., Araújo, L. R., Alves, E. O., Batista, P. P., & Clemesha, B. R. (2015). Variations in meteor heights at 22.7°S during solar cycle 23. *Journal of Atmospheric and Solar-Terrestrial Physics*, *133*, 139–144. https://doi.org/10.1016/j.jastp.2015.08.015

Liu, A. Z., Lu, X., & Franke, S. J. (2013). Diurnal variation of gravity wave momentum flux and its forcing on the diurnal tide. *Journal of Geophysical Research: Atmospheres*, *118*(4), 1668–1678. https://doi.org/10.1029/2012JD018653

Liu, X., Yue, J., Xu, J., Garcia, R. R., Russell, J. M., III., Mlynczak, M., et al. (2017). Variations of global gravity waves derived from 14 years of SABER temperature observations. *Journal of Geophysical Research: Atmospheres*, *122*(12), 6231–6249. https://doi.org/10.1002/2017JD026604

Lübken, F.-J., & Berger, U. (2011). Latitudinal and interhemispheric variation of stratospheric effects on mesosphere ice layer trends. *Journal of Geophysical Research*, *116*, D4. https://doi.org/10.1029/2010JD015258

Lübken, F.-J., Berger, U., & Baumgarten, G. (2009). Stratospheric and solar cycle effects on long-term variability of mesospheric ice clouds. *Journal of Geophysical Research*, *114*, D1. https://doi.org/10.1029/2009JD012377

Lübken, F.-J., Berger, U., & Baumgarten, G. (2013). Temperature trends in the midlatitude summer mesosphere. *Journal of Geophysical Research: Atmospheres*, *118*(24), 13347–13360. https://doi.org/10.1002/2013JD020576

Marsh, D. R., Garcia, R. R., Kinnison, D. E., Boville, B. A., Sassi, F., Solomon, S. C., & Matthes, K. (2007). Modeling the whole atmosphere response to solar cycle changes in radiative and geomagnetic forcing. *Journal of Geophysical Research*, *112*(D23), D23396. https://doi.org/10.1029/2006JD008306

Mlynczak, M. G., Hunt, L., Garcia, R. R., Harvey, V. L., Marshall, B. T., Yue, J., et al. (2022). Cooling and contraction of the mesosphere and lower thermosphere from 2002 to 2021. *Journal of Geophysical Research: Atmospheres*, *127*(22), e2022JD036767. https://doi.org/10.1029/2022JD036767

Mlynczak, M. G., Hunt, L. A., Marshall, B. T., Martin-Torres, F. J., Mertens, C. J., Russell, J. M., III, et al. (2010). Observations of infrared radiative cooling in the thermosphere on daily to multiyear timescales from the TIMED/SABER instrument. *Journal of Geophysical Research*, *115*(A3). https://doi.org/10.1029/2009JA014713

Nedoluha, G. E., Gomez, R. M., Hicks, B. C., Wrotny, J. E., Boone, C., & Lambert, L. (2009). Water vapor measurements in the mesosphere from Mauna Loa over solar cycle, 23. *Journal of Geophysical Research*, *114*(D23), D23303. https://doi.org/10.1029/2009JD012504

Offerman, D., Hoffman, P., Knieling, P., Koppmann, R., Oberheide, J., & Steinbrecht, W. (2010). Long-term trends and solar cycle variations of mesospheric temperature and dynamics. *Journal of Geophysical Research*, *115*, D18. https://doi.org/10.1029/2009JD013363

Plane, J. M. C., Feng, W., & Dawkins, E. C. M. (2015). The mesosphere and metals: Chemistry and changes. *Chemical Reviews*, *115*(10), 4497–4541. https://doi.org/10.1021/cr500501m

Qian, L., Burns, A. G., Solomon, S. C., & Wang, W. (2017). Carbon dioxide trends in the mesosphere and lower thermosphere. *Journal of Geophysical Research: Space Physics*, *122*(4), 4474–4488. https://doi.org/10.1002/2016JA023825

Qian, L., Jacobi, C., & McInerney, J. (2019). Trends and solar irradiance effects in the mesosphere. *Journal of Geophysical Research: Space Physics*, *124*(2), 1343–1360. https://doi.org/10.1029/2018JA026367

Qian, L., Laštovička, J., Roble, R. G., & Solomon, S. C. (2011). Progress in observations and simulations of global change in the upper atmosphere. *Journal of Geophysical Research*, *116*(A2). https://doi.org/10.1029/2010JA016317

Randel, W. J., Polvani, L., Wu, F., Kinnison, D. E., Zou, C.-Z., & Mears, C. (2017). Troposphere-stratosphere temperature trends derived from satellite data compared with ensemble simulations from WACCM. *Journal of Geophysical Research: Atmospheres*, *122*(18), 9651–9667. https://doi.org/10.1002/2017JD027158

Remsberg, E. (2008). On the observed changes in upper stratospheric and mesospheric temperatures from UARS HALOE. *Annales Geophysicae*, *26*(5), 1287–1297. https://doi.org/10.5194/angeo-26-1287-2008

Remsberg, E., Damadeo, R., Natarajan, M., & Bhatt, P. (2018). Observed responses of mesospheric water vapor to solar cycle and dynamical forcings. *Journal of Geophysical Research: Atmospheres*, *123*(7), 3830–3843. https://doi.org/10.1002/2017JD028029

Roble, R. G. (1995). Major greenhouse cooling (yes, cooling): The upper atmosphere response to increased CO_2. *Review of Geophysics*, *33*(S1), 539–546. https://doi.org/10.1029/95RG00118

Roble, R. G., & Dickinson, R. E. (1989). How will changes in carbon dioxide and methane modify the mean structure of the mesosphere and thermosphere? *Geophysical Research Letters*, *16*(12), 1441–1444. https://doi.org/10.1029/GL016i012p01441

Sharma, S., Kumar, P., Vaishnav, R., Jethva, C., & Bencherif, H. (2018). Evaluation of inter-hemispheric characteristics of tropopause-stratopause-mesopause over sub-Tropical regions. *Pure and Applied Geophysics*, *175*(3), 1123–1137. https://doi.org/10.1007/s00024-017-1706-8

Shettle, E. P., DeLand, M. T., Thomas, G. E., & Olivero, J. J. (2009). Long term variations in the frequency of polar mesospheric clouds in the Northern Hemisphere from SBUV. *Geophysical Research Letters*, *36*(2). https://doi.org/10.1029/2008GL036048

Smith-Johnson, C., Marsh, D. R., Smith, A. K., Tyssøy, H. N., & Maliniemi, V. (2022). Mesospheric nitric oxide transport in WACCM. *Journal of Geophysical Research: Space Physics*, *127*(3), e2021JA029998. https://doi.org/10.1029/2021JA029998

Solomon, S. C., Liu, H.-L., Marsh, D. R., McInerney, J. M., Qian, L., & Vitt, F. M. (2019). Whole atmosphere climate change: Dependence on solar activity. *Journal of Geophysical Research: Space Physics*, *124*(5), 3799–3809. https://doi.org/10.1029/2019ja026678

Sparks, J. J., & Janches, D. (2009). Correction to "Latitudinal dependence of the variability of the micrometeor altitude distribution". *Geophysical Research Letters*, *36*(17), L17101. https://doi.org/10.1029/2009gl039987

Stober, G., Liu, A., Kozlovsky, A., Qiao, Z., Kuchar, A., Jacobi, C., et al. (2022). Meteor radar vertical wind observation biases and mathematical debiasing strategies including a 3DVAR+DIV algorithm. *Atmospheric Measurement Techniques*, *15*(19), 5769–5792. https://doi.org/10.5194/egusphere-2022-203

Stober, G., Matthias, V., Brown, P., & Chau, J. L. (2014). Neutral density variation from specular meteor echo observations spanning one solar cycle. *Geophysical Research Letters*, *41*(19), 6919–6925. https://doi.org/10.1002/2014GL061273

Vincent, R. A. (2015). The dynamics of the mesosphere and lower thermosphere: A brief review. *Progress in Earth and Planetary Science*, *2*(4), 4. https://doi.org/10.1186/s40645-015-0035-8

Vorobeva, E. (2019). Notes on the correlation between sudden stratospheric warmings and solar activity. *Annales Geophysicae*, *37*(3), 375–380. https://doi.org/10.5194/angeo-37-375-2019

Wilhelm, S., Stober, G., & Brown, P. (2019). Climatologies and long-term changes in mesospheric wind and wave measurements based on radar observations at high and mid latitudes. *Annales Geophysicae*, *37*(5), 851–875. https://doi.org/10.5194/angeo-37-851-2019

Xu, J., Smith, A. K., Yuan, W., Liu, H.-L., Wu, Q., Mlynczak, M. G., & Russell, J. M., III. (2007). Global structure and long-term variations of zonal mean temperature observed by TIMED/SABER. *Journal of Geophysical Research*, *112*, D24. https://doi.org/10.1029/2007JD008546

Yuan, T., Solomon, S. C., She, C.-Y., Krueger, D. A., & Liu, H.-L. (2019). The long-term trends of nocturnal mesopause temperature and altitude revealed by Na lidar observations between 1990 and 2018 at midlatitude. *Journal of Geophysical Research: Atmospheres*, *124*(12), 5970–5980. https://doi.org/10.1029/2018JD029828

Zhao, X. R., Sheng, Z., Shi, H. Q., Weng, L. B., & He, Y. (2021). Middle atmosphere temperature changes derived from SABER observations during 2002-20. *Journal of Climate*, *34*(19), 7995–8012. https://doi.org/10.1175/JCLI-D-20-1010.1

Zhao, X. R., Sheng, Z., Shi, H. Q., Weng, L. B., & Liao, Q. X. (2020). Long-term trends and solar response of the mesopause temperatures observed by SABER during the 2002-2019 period. *Journal of Geophysical Research: Atmospheres*, *125*(11), e2020JD032418. https://doi.org/10.1029/2020JD032418